ADVANCED ENERGY MATERIALS
www.advenergymat.de

Cycling Performance and Mechanistic Insights of Ferricyanide Electrolytes in Alkaline Redox Flow Batteries

*Maowei Hu, Abigail P. Wang, Jian Luo, Qianhusn Wei, and T. Leo Liu**

Ferrocyanide, such as $K_4[Fe(CN)_6]$, is one of the most popular cathode electrolyte (catholyte) materials in redox flow batteries. However, its chemical stability in alkaline redox flow batteries is debated. Mechanistic understandings at the molecular level are necessary to elucidate the cycling stability of $K_4[Fe(CN)_6]$ and its oxidized state ($K_3[Fe(CN)_6]$) based electrolytes and guide their proper use in flow batteries for energy storage. Herein, a suite of battery tests and spectroscopic studies are presented to understand the chemical stability of $K_4[Fe(CN)_6]$ and its charged state, $K_3[Fe(CN)_6]$, at a variety of conditions. In a strong alkaline solution (pH 14), it is found that the balanced $K_4[Fe(CN)_6]/K_3[Fe(CN)_6]$ half-cell experiences a fast capacity decay under dark conditions. The studies reveal that the chemical reduction of $K_3[Fe(CN)_6]$ by a graphite electrode leads to the charge imbalance in the half-cell cycling and is the major cause of the observed capacity decay. In addition, at pH 14, $K_3[Fe(CN)_6]$ undergoes a slow CN^-/OH^- exchange reaction. The dissociated CN^- ligand can chemically reduce $K_3[Fe(CN)_6]$ to $K_4[Fe(CN)_6]$ and it is converted to cyanate (OCN^-) and further, decomposes into CO_3^{2-} and NH_3. Ultimately, the irreversible chemical conversion of CN^- to OCN^- leads to the irreversible decomposition of $K_4/K_3[Fe(CN)_6]$ at pH 14.

1. Introduction

Aqueous organic/organometallic redox flow batteries (AORFBs) are considered promising technologies for scalable, long-duration energy storage.[1,2] The most attractive merits of AORFBs arise from the sustainability and structural tunability of redox-active organic and organometallic molecules.[1] Particularly, the structural tunability can enable desired performance metrics at the electrolyte materials level for energy storage, including optimal redox potential, high capacity, high conductivities, durability, and low permeability.[1] In the past decade, a number of privileged redox active molecules have been identified and optimized as charge storage electrolyte materials in AORFBs, e.g., viologen,[3–5] anthraquinone,[6,7] and phenazine[8,9] based anolytes, and ferrocene,[10–12] 2,2,6,6-Tetramethylpiperidin-1-yl)oxyl,[13,14] and ferrocyanide[15] based catholytes.

Compared to the well-established cycling stability of viologen, anthraquinone, and phenazine organic anolytes, the lack of stable, capacity-dense organic and organometallic catholytes is a serious challenge for AORFBs.[16,17] Ferrocyanide, such as $K_4[Fe(CN)_6]$, is the most frequently used cathode electrolyte material in alkaline redox flow batteries.[17] However, the chemical stability of potassium ferrocyanide ($K_4[Fe(CN)_6]$) and its oxidized state ($K_3[Fe(CN)_6]$) in alkaline redox flow batteries have received debate in recent publications.[18–22] We first reported the cycling stability of $K_4[Fe(CN)_6]$ in pH neutral and alkaline conditions using a balanced half-cell approach (**Figure 1**A) and revealed the fast capacity decay of a $K_4[Fe(CN)_6]/K_3[Fe(CN)_6]$ half-cell at alkaline conditions.[18] However, unbalanced $K_4[Fe(CN)_6]/K_3[Fe(CN)_6]$ alkaline half-cell flow battery studies (Figure 1B) by other groups suggested that the chemical stability issue of potassium ferrocyanide and potassium ferricyanide is not concerned in alkaline solutions.[19,20] Different from a balanced half-cell (Figure 1A), the volume (Figure 1B,C) or concentration of a discharged electrolyte and a charged electrolyte is different in an unbalanced half-cell.[16] The contradicting results reported by different studies and the lack of molecule-level understanding in previous studies encourage us to conduct an in-depth mechanistic study of potassium ferrocyanide and potassium ferricyanide in alkaline flow batteries. Through a suite of battery testing, spectroscopic studies, and isotope labeling experiments, we elucidated the chemical redox and ligand dissociation degradation mechanisms of the ferricyanide (charged state) under alkaline conditions and also characterized a number of degradation products of the cyanide ligand dissociated from ferricyanide and graphite electrodes. Our results confirm that ferrocyanide is best used at pH neutral and near neutral conditions instead of strong alkaline conditions. In addition, this work also stresses the proper use of the half-cell approach to evaluating the cycling stability of a redox electrolyte. The presented study is highly valuable to guide the evaluation of energy storage performance and mechanistic understanding of other redox electrolytes and develop advanced redox electrolytes for scalable, long-duration energy storage.

M. Hu, A. P. Wang, J. Luo, Q. Wei, T. L. Liu
Department of Chemistry and Biochemistry
Utah State University
Logan, UT 84322, USA
E-mail: leo.liu@usu.edu

The ORCID identification number(s) for the author(s) of this article can be found under https://doi.org/10.1002/aenm.202203762.

DOI: 10.1002/aenm.202203762

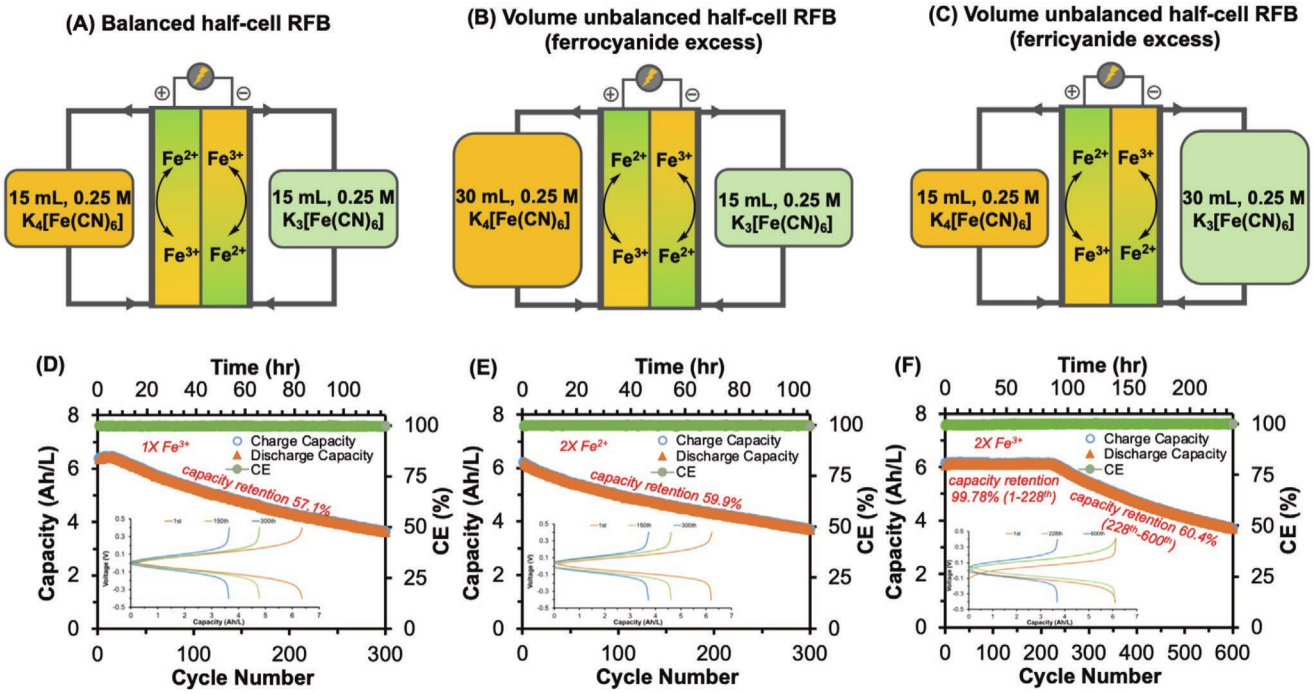

Figure 1. Schematic illustrations and cycling performance of the $K_4[Fe(CN)_6]/K_3[Fe(CN)_6]$ half-cell using $K_4[Fe(CN)_6]$ (discharged state) and $K_3[Fe(CN)_6]$ (charged state) electrolytes at pH 14. A) Balanced half-cell; B) volume unbalanced half-cell with ferrocyanide excess; C) volume unbalanced half-cell with ferricyanide excess; D) a balanced half-cell: 15 mL, 0.25 m $K_4[Fe(CN)_6]$, and 15 mL, 0.25 m $K_3[Fe(CN)_6]$; E) a volume unbalanced half-cell: 30 mL, 0.25 m $K_4[Fe(CN)_6]$, and 15 mL, 0.25 m $K_3[Fe(CN)_6]$; and F) a volume unbalanced half-cell: 15 mL, 0.25 m $K_4[Fe(CN)_6]$, and 30 mL, 0.25 m $K_3[Fe(CN)_6]$.

2. Results and Discussion

2.1. Half-Cell Studies of $K_4[Fe(CN)_6]/K_3[Fe(CN)_6]$

We set out to systematically compare the cycling performance of $K_4[Fe(CN)_6]/K_3[Fe(CN)_6]$ half-cells using 1.0 m KOH supporting electrolyte (pH 14) under balanced and nonbalanced cell conditions (Figure 1). To avoid the light impact, except as mentioned, cycling studies were conducted in a nitrogen glovebox under dark conditions at room temperature.[11] The effect of ambient light will be discussed in the later section separately. A 15 mL, 0.25 m balanced $K_4[Fe(CN)_6]/K_3[Fe(CN)_6]$ half-cell displayed total capacity retention of about 57.1% (or 99.858%/cycle) for 300 cycles or 99.634% h^{-1}. An unbalanced half-cell consisting of 30 mL, 0.25 m $K_4[Fe(CN)_6]$ and 15 mL, 0.25 m $K_3[Fe(CN)_6]$ exhibited comparable capacity retention of 59.9% after 300 cycles. In stark contrast, a second unbalanced half-cell with 15 mL, 0.25 m $K_4[Fe(CN)_6]$ and 30 mL, 0.25 m $K_3[Fe(CN)_6]$ (Figure 1F) demonstrated fairly stable cycling for 228 cycles, capacity retention of 99.76% for 228 cycles (99.998% per cycle or 99.996% h^{-1}) and then started to show quick capacity decay for the rest of 372 cycles, total capacity retention of 60.4% (99.894% per cycle or 99.727% h^{-1}). Collectively, these results suggest that the cycling stability of the $K_4[Fe(CN)_6]/K_3[Fe(CN)_6]$ half-cell was not apparently influenced by the capacity of $K_4[Fe(CN)_6]$ but was significantly limited by the capacity of $K_3[Fe(CN)_6]$. In the third half-cell, excess $K_3[Fe(CN)_6]$ is believed to compensate for the degradation of the charged state, $K_3[Fe(CN)_6]$. Until 228 cycles, the excess $K_3[Fe(CN)_6]$ was consumed and the capacity decay of the half-cell became observable as the first two half-cells (Table S1, Supporting Information, shows the details of cycling stability).

For comparison, we investigated the cycling stability of the $K_4[Fe(CN)_6]/K_3[Fe(CN)_6]$ half-cell at pH 7 under the same conditions. Specifically, a balanced 0.25 m $K_4[Fe(CN)_6]/K_3[Fe(CN)_6]$ half-cell delivered near 100% capacity retention at pH 7 (**Figure 2** and Table S1, Supporting Information) for 300 cycles. Consistent with our earlier work,[18] the cycling stability of the $K_4[Fe(CN)_6]/K_3[Fe(CN)_6]$ half-cell is strongly pH dependent.

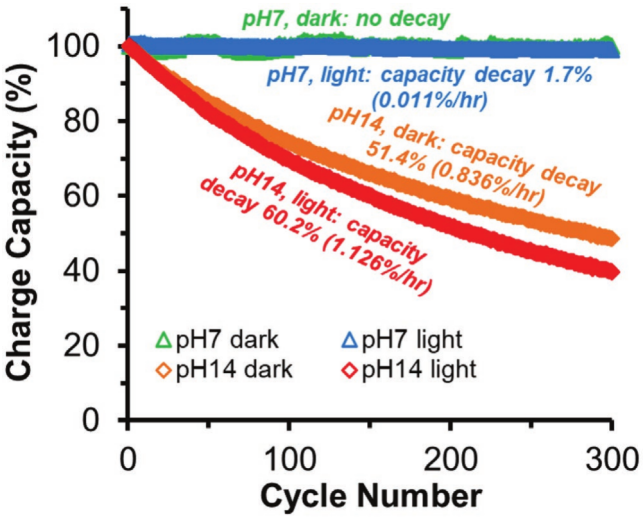

Figure 2. Cycling performance of the $K_4[Fe(CN)_6]/K_3[Fe(CN)_6]$ half-cell at different conditions.

2.2. Spectroscopic Studies to Understand the Stability of $K_3[Fe(CN)_6]$ and $K_4[Fe(CN)_6]$

To gain a further understanding of the chemical stability of $K_4[Fe(CN)_6]$ and $K_3[Fe(CN)_6]$ under alkaline conditions, UV–vis spectroscopic studies were conducted before and after battery cycling for the balanced $K_4[Fe(CN)_6]/K_3[Fe(CN)_6]$ half-cell (**Figure 3**A). To avoid possible contamination by air, samples for spectroscopic studies were prepared under a nitrogen atmosphere. For the $K_3[Fe(CN)_6]$ electrolyte, the degradation was indicated by the decrease of the absorption at 421 nm (47.1%). Only a very minor decrease at 324 nm was observed for the $K_4[Fe(CN)_6]$ electrolyte. These results suggest the stability of $K_3[Fe(CN)_6]$ is the major concern for the battery capacity decay. Thus, ensuing studies mainly focused on $K_3[Fe(CN)_6]$.

Control experiments were conducted to understand the degradation of $K_3[Fe(CN)_6]$. 0.25 m $K_3[Fe(CN)_6]$ at the pH 14 solutions were circulated without electrochemical cycling to mimic the battery test, only with a piece of graphite felt or only with a graphite chamber under flow conditions. UV–vis and IR studies were performed to monitor the status of the electrolytes for 6 d. Similar results were obtained in UV–vis studies (Figures S1–S5, Supporting Information). In the IR studies (Figure 3B), it was found that the concentration of $K_3[Fe(CN)_6]$ with a CN stretch at 2115 cm^{-1} kept decreasing, i.e., about 0.1 m after 6 d compared to the initial 0.25 m. In the meanwhile, the appearance of $K_4[Fe(CN)_6]$ was evidently observed at 2038 cm^{-1} with a concentration of about 0.14 m after 6 d. The IR results reveal that $K_3[Fe(CN)_6]$ undergoes a chemical redox reaction to form $K_4[Fe(CN)_6]$.

The chemical stability of $K_4[Fe(CN)_6]$ (0.2 mm) and $K_3[Fe(CN)_6]$ (0.2 mm) were further studied by UV–vis in vials at a variety of conditions. In the presence of graphite felt, the solution of $K_3[Fe(CN)_6]$ (0.2 mm) exhibited a quick decay only in a few hours (Figure 3C,D) with a $t_{1/2}$ of ≈3 h. Even without graphite felt, $K_3[Fe(CN)_6]$ also exhibited slower but substantial degradation in 3 weeks with a $t_{1/2}$ of ≈2 weeks (blue triangle curve in Figure 3D and also see Figure S6, Supporting Information). No apparent spectroscopic change was observed for $K_4[Fe(CN)_6]$ (Figure S7, Supporting Information). In stark contrast, at pH 7, nearly no degradation was observed for $K_3[Fe(CN)_6]$ with and without graphite felt (circle curves in Figure 3D) up to 21 d. These results further confirm that the chemical reduction of $K_3[Fe(CN)_6]$ to $K_4[Fe(CN)_6]$ occurs at pH 14 and is significantly accelerated by a carbon material, graphite felt or a graphite chamber.

According to the above pH dependence studies, the observed chemical reduction of $K_3[Fe(CN)_6]$ to $K_4[Fe(CN)_6]$ suggests that hydroxide (HO^-) acts as a reactant at pH 14 to trigger the chemical redox reaction. Under strong alkaline conditions, one might think the oxygen evolution reaction, i.e., the oxidation of OH^- by $K_3[Fe(CN)_6]$, might be the cause of the chemical redox reaction.[19,20,22] The graphite felt electrode was proposed as a catalyst for the oxidation of OH^-.[22] To verify this possibility, careful tests

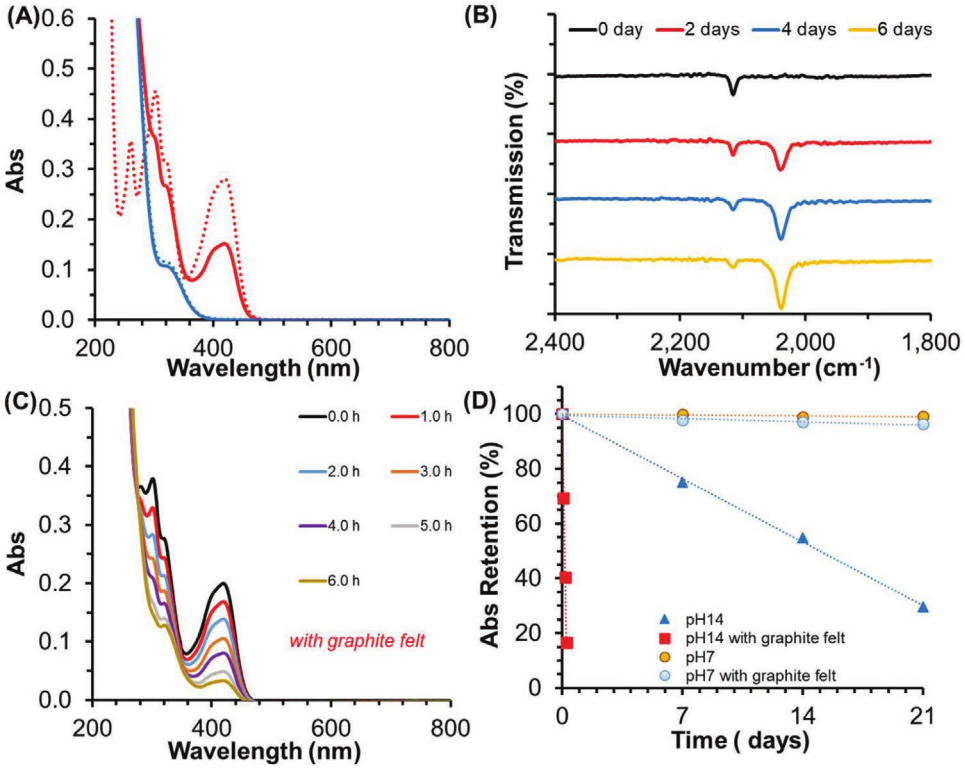

Figure 3. UV–vis and IR monitor the $K_3[Fe(CN)_6]$ and $K_4[Fe(CN)_6]$ electrolytes under cycling and noncycling conditions at pH 14. A) UV–vis studies of $K_3[Fe(CN)_6]$ (red curves) and $K_4[Fe(CN)_6]$ (blue curves) before (dotted curves) and after (line curves) cycling. B) IR studies of a 0.25 m $K_3[Fe(CN)_6]$ electrolyte circulated through a piece of graphite felt or a graphite chamber. C) UV–vis studies of 0.2 mm $K_3[Fe(CN)_6]$ in a vial in the presence of a piece of graphite felt. D) Stability comparison of $K_3[Fe(CN)_6]$ at pH 7 and pH 14 with and without a piece of graphite felt.

for the headspace of 0.25 m $K_3[Fe(CN)_6]$ at pH 14 solution stirred with or without a graphite felt electrode in the Ar glovebox were conducted to identify O_2 formation. gas chromatography with thermal conductivity detection tests revealed negligible O_2 formation under both conditions. The calculated amount of O_2 using a standard curve is counted as less than 1% of the total electron for the chemical redox reaction of $K_3[Fe(CN)_6]$ to $K_4[Fe(CN)_6]$ even with graphite felt (see details in the Supporting Information, Figures S8–S10, Supporting Information). It is also noted that the GC results from an independent study by Aziz's group also only detected a very weak peak of O_2.[22] In their work, the amount of O_2 was not quantified. In addition, a clear CO signal was detected by gas chromatography with flame ionization detection (GC-FID) in the headspace of the $K_3[Fe(CN)_6]$ solution at pH 14 in the presence of graphite felt, which was incorrectly assigned as NH_3 in our original ChemRxiv preprint.[21] The concentration of generated CO was also calculated below 1% of the electron contribution (see details in the Supporting Information, Figures S12 and S13, Supporting Information). Without the graphite felt, CO was not detected by GC-FID (Figure S14, Supporting Information). It is believed that CO was generated by the oxidation of graphite felt under strongly alkaline conditions. GC-FID tests from the battery cycling conditions gave similar results (Figure S11, Supporting Information).

Based on the above results, either O_2 or CO generation only contributes a very small portion of electrons to reduce $K_3[Fe(CN)_6]$ (less than 2% electrons in total compared to the capacity loss). Then we conducted NMR studies to identify other possible degradation products. Two peaks at 169.25 and 174.34 ppm were observed in the ^{13}C NMR spectrum of the cycled $K_4[Fe(CN)_6]$ electrolyte (**Figure 4**A). According to several standard samples of possible carbon-based compounds (Table S2, Supporting Information), the peak at 169.25 ppm is assigned to CO_3^{2-}, and the smaller peak at 174.34 ppm is assigned to formate. Based on a standard test of the carbonate, the concentration of the carbonate in the cycled $K_4[Fe(CN)_6]$ electrolyte is ≈0.04 m (Figure S19, Supporting Information). If assuming the two-electron formation of the carbonate (C^{4+}) from a C^{2+} precursor, the estimated amount of the carbonate roughly corresponds to about 75% (≈0.08 m) of the capacity loss of $K_4[Fe(CN)_6]/K_3[Fe(CN)_6]$ half-cell at pH 14 (Figure 1D, the capacity decay is 42.9% in 0.25 m pH 14 battery). The other electron loss (≈25%) might be due to other products (such as

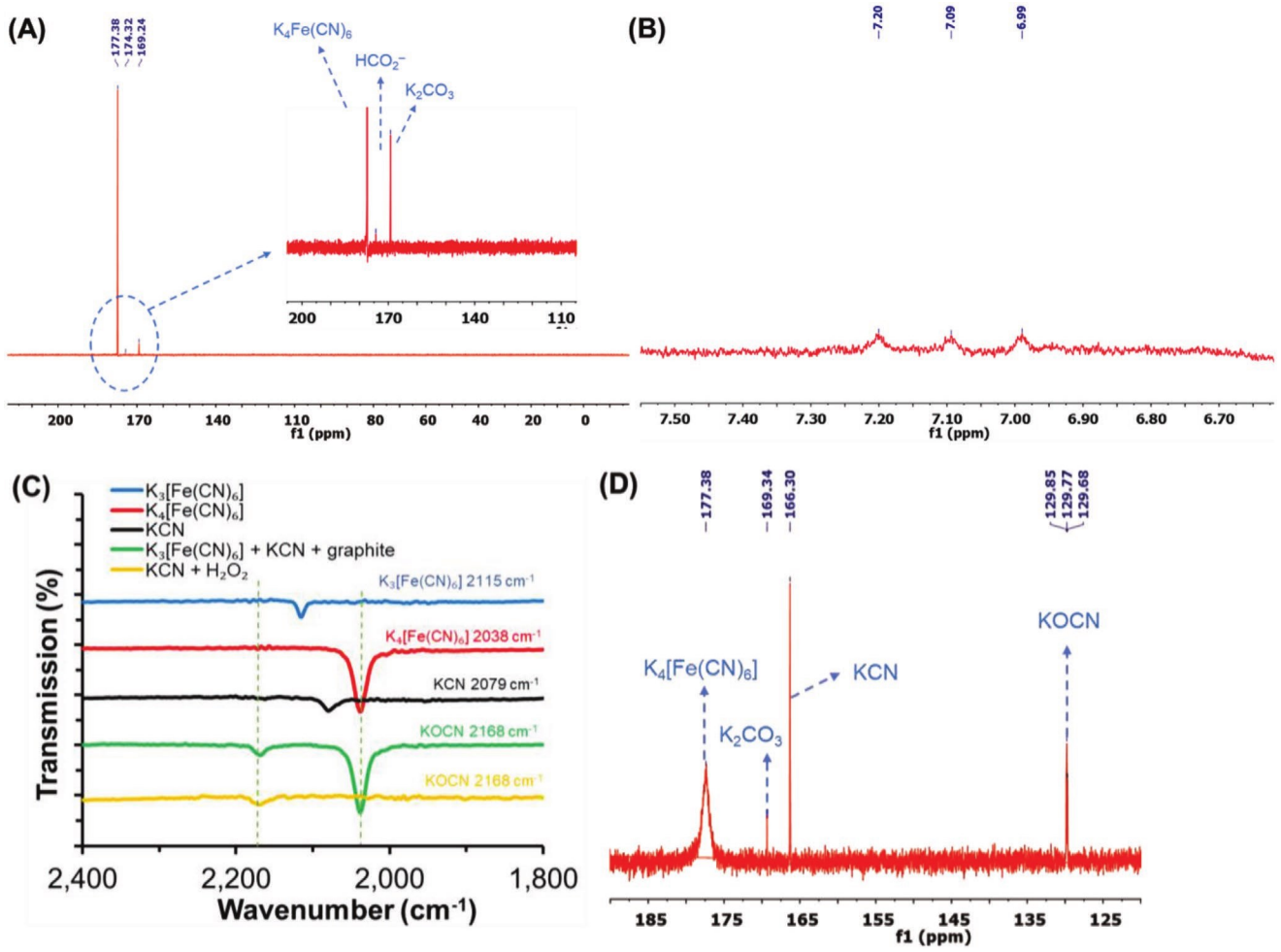

Figure 4. Spectroscopic studies of the $K_3[Fe(CN)_6]$ electrolyte. A) ^{13}C NMR of 0.25 m $K_4[Fe(CN)_6]/K_3[Fe(CN)_6]$ half-cell battery after cycling at pH 14 under dark. B) ^{1}H NMR of 0.25 m $K_4[Fe(CN)_6]/K_3[Fe(CN)_6]$ half-cell battery after cycling at pH14 under dark after adding HCl. C) IR monitor of the chemical redox reaction of $K_3[Fe(CN)_6]$ and KCN at pH 14. D) ^{13}C NMR spectrum of the reaction solution of $K_3[Fe(CN)_6]$ and KCN at pH 14.

formate, not counted) or insoluble compounds formed on the surface of the graphite electrode. In addition, ammonium was observed in the ^{1}H NMR spectrum after the cycled $K_3[Fe(CN)_6]$ electrolyte was treated with HCl (Figure 4B). More discussions about ammonium formation are provided below. A control experiment of graphite alone in 1.0 m KOH did not detect the signals for carbonate in the ^{13}C NMR and ammonium the ^{1}H NMR spectrum under N_2, ruling out the contamination of K_2CO_3 and ammonium from starting materials and/or the experiment environment (Figures S15–S18, Supporting Information). It should be noted that carbonate was formed by the direct capture of CO_2 after exposure of a KOH solution to air for one week but not for a KOH solution under N_2 (Figure S18, Supporting Information).

2.3. Understanding CN Ligand Dissociation of $K_3[Fe(CN)_6]$ and Subsequent Degradation

As $K_3[Fe(CN)_6]$ displayed slow degradation even without the graphite felt (Figure 3D and Figure S6, Supporting Information), we suspected that under highly basic conditions, ligand exchange from CN^- to OH^- might occur for $K_3[Fe(CN)_6]$. Our recent studies revealed that ferrocene electrolytes undergo ligand dissociation to cause a capacity loss in flow batteries, a legit degradation passway for organometallic molecules.[11] The dissociated cyanide (CN^-) ligands might be a reductant to reduce $K_3[Fe(CN)_6]$.[23] The addition of KCN to 0.25 m $K_3[Fe(CN)_6]$ at pH 14 led to clear color fading from green to light orange. The IR test shows the formation of $K_4[Fe(CN)_6]$ within a few hours (Figure 4C, green curve). A new peak at 2168 cm^{-1} appeared and is assigned to potassium cyanate (Figure 4C, green curve), the oxidized product of KCN by $K_3[Fe(CN)_6]$ in the presence of hydroxide. This was further confirmed by the oxidation of KCN by adding H_2O_2 (Figure 4C, yellow curve). The reaction solution was further studied using NMR. In the ^{13}C NMR spectra (Figure 4D), $K_4[Fe(CN)_6]$ (177.38 ppm), potassium cyanate (KOCN) (129.97 ppm, Figure S20, Supporting Information), KCN (166.30 ppm, Table S2, Supporting Information), and a peak of carbonate at 169.34 ppm were observed. This means dissociated free CN^- will be oxidized to OCN^- by $K_3[Fe(CN)_6]$ in the solution. Further studies also found that KOCN at pH 14 could easily decompose to K_2CO_3 (Figure S21, Supporting Information). It is noted that KOCN was not observed in the cycled $K_3[Fe(CN)_6]$ electrolyte. It is possible that the concentration of KOCN under the electrochemical cycling conditions is too low to be detected as it could undergo further decomposition to K_2CO_3, which was verified by isotope labeling studies (see below).

It is worth noting that the ammonium peak was also found from the mixture solution of $K_3[Fe(CN)_6]$ and KCN (Figure S22, Supporting Information) after acid treatment. Parallel control experiments were conducted by using fresh 0.25 m $K_4[Fe(CN)_6]$ and $K_3[Fe(CN)_6]$ at pH 14 instead of battery post-cycling electrolyte (Figures S23 and S24, Supporting Information), no ammonium was found. No ammonium peak was found in $K_4[Fe(CN)_6]$ and $K_4[Fe(CN)_6]$ solutions up to 24 h (Figures S25 and S26, Supporting Information). These control experiments rule out the ammonium formation directly from the decomposition of $K_4[Fe(CN)_6]$ or $K_3[Fe(CN)_6]$ under acidic conditions. Thus, it is believed that ammonia (NH_3) is a further decomposition product from KOCN. One needs to be careful as that $K_4[Fe(CN)_6]$ and $K_3[Fe(CN)_6]$ are not stable in acidic conditions and decompose to release highly toxic hydrogen cyanide and form a Prussian blue precipitate.

2.4. Isotope Labeling Studies Using $K_4[Fe(^{13}CN)_6]$ and $K_4[Fe(C^{15}N)_6]$

To further confirm the decomposition pathway of the CN ligand, ^{13}C labeled $K_4[Fe(^{13}CN)_6]$ and ^{15}N labeled $K_4[Fe(C^{15}N)_6]$ were synthesized from $K^{13}CN$ and $KC^{15}N$ with $FeCl_2$ separately (Figures S28–S31, Supporting Information). Then 0.1 m $K_4[Fe(^{13}CN)_6]$ and $K_4[Fe(C^{15}N)_6]$ at pH 14 were oxidized electrochemically to corresponding $K_3[Fe(^{13}CN)_6]$ and $K_3[Fe(C^{15}N)_6]$, respectively. 0.1 m $K_4[Fe(^{13}CN)_6]/K_3[Fe(CN)_6]$ and $K_3[Fe(C^{15}N)_6]/K_3[Fe(CN)_6]$ half-cells were cycled until the loss of full capacity after 3 d. ^{13}C NMR spectra were recorded for $K_4[Fe(^{13}CN)_6]$ before and after cycling in a flow battery. Besides the decomposed product of K_2CO_3, a small triplet peak belonging to $KO^{13}CN$ could be observed in the solution, which benefitted from a 100% abundance of ^{13}C to detect a low concentration of KOCN (**Figure 5**A and Figure S33, Supporting Information). The stretch of OCN^- was also detected in an alkaline $K_3[Fe(CN)_6]$ electrolyte after more than 4 months of cycling in a previous study.[24] However, it was assigned as the stretch of the bridge CN^- of a dimer Fe^{3+} compound. These experimental results confirmed the conversion from the dissociated CN^- to OCN^- and finally to CO_3^{2-} as observed by ^{13}C NMR. An independent ^{13}C NMR study confirmed the conversion of OCN^- to CO_3^{2-} at pH 14 (Figure S21, Supporting Information). The ^{1}H NMR studies of the cycled $K_4[Fe(C^{15}N)_6]$ solution after the treatment of HCl disclosed a doublet peak belonging to $^{15}NH_4^+$ (Figure 5B), further confirming its origin coming from the dissociated $C^{15}N^-$ of the $K_3[Fe(C^{15}N)_6]$ in strongly alkaline conditions. Similar results from the solutions of $K_3[Fe(^{13}CN)_6]$ and $K_3[Fe(C^{15}N)_6]$ with a piece of graphite felt were obtained.

In the ^{13}C NMR spectra, the integration of the CO_3^{2-} peak of the cycled $K_4[Fe(^{13}CN)_6]$ has a comparable concentration with nonlabeling $K_4[Fe(CN)_6]$ using an internal standard (Figure S38, Supporting Information). This result suggests that only a small portion of CO_3^{2-} comes from the decomposition of $KO^{13}CN$ originated from $K_4[Fe(^{13}CN)_6]$. In addition, it is noted that a dominant triplet peak of $^{14}NH_4^+$ was observed in the ^{1}H NMR spectrum of the $K_3[Fe(C^{15}N)_6]$ solution and is about ten times of the observed $^{15}NH_4^+$, which was not generated from $K_3[Fe(C^{15}N)_6]$. It is believed that dominant CO_3^{2-} and $^{14}NH_4^+$ come from the chemical oxidation of the graphite felt electrode by $K_3[Fe(CN)_6]$. This explanation is consistent with the chemical stability of $K_3[Fe(CN)_6]$ with and without graphite.

2.5. Reuse of Graphite Electrodes in $K_4[Fe(CN)_6]/K_3[Fe(CN)_6]$ Half-Cells at pH 14

Graphite felt was widely used as an electrode in redox flow batteries; however, its chemical stability in alkaline conditions has

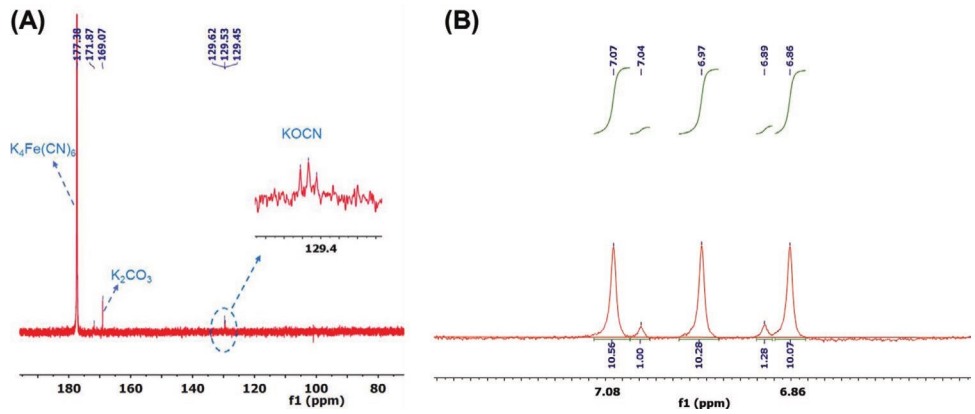

Figure 5. NMR spectra of isotope labeling studies. A) ^{13}C NMR of 0.1 m $K_4[Fe(^{13}CN)_6]/K_3[Fe(CN)_6]$ half-cell battery after cycling at pH 14 under dark (4096 scans, 4 s delay). B) ^1H NMR of 0.1 m $K_4[Fe(C^{15}N)_6]/K_3[Fe(CN)_6]$ half-cell battery after cycling at pH 14 under dark (256 scans, 2 s delay).

not received enough attention in flow battery studies. An energy dispersive spectroscopy (EDS) mapping test found C, N, S, Fe, and other elements co-exist in the graphite felt electrode (Figure S39, Supporting Information). To further verify the effect of the graphite electrode, a series of 0.25 m $K_3[Fe(CN)_6]/K_4[Fe(CN)_6]$ balanced half-cells, as aforementioned (Figure 1) was tested at pH 14. The graphite felt electrode was reused three times, and each time a new battery was built with the same concentration of fresh solutions. As seen in **Figure 6**, the batteries showed improved stability after using the used graphite felt electrodes, which confirms chemical changes of the graphite felt electrodes. The improved performance gives a clue that maybe the consumption of reductive functional groups on the graphite felt electrode surface mitigates the battery capacity decay. The ^{13}C NMR was recorded after the 2nd and 3rd reuse of the graphite electrodes, and a similar amount of CO_3^{2-} was found in both electrolytes (Figure S40, Supporting Information).

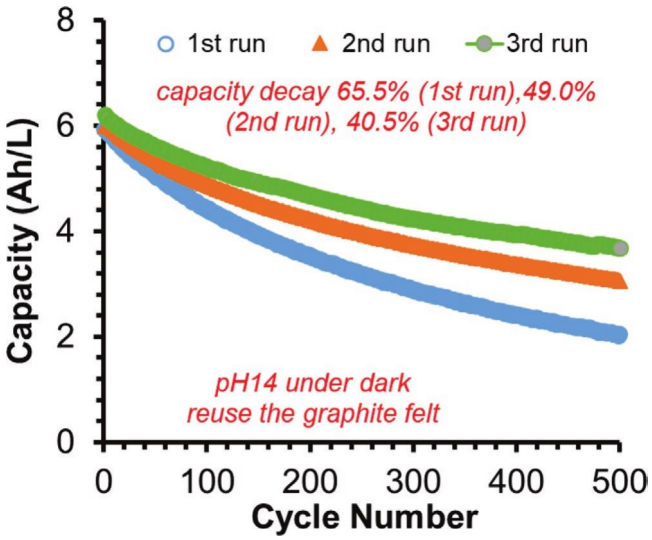

Figure 6. Cycling comparison of 0.25 m $K_4[Fe(CN)_6]/K_3[Fe(CN)_6]$ balanced half-cells at pH 14 by reusing the graphite felt electrodes.

2.6. Proposed Degradation Mechanisms of $K_3[Fe(CN)_6]$ at pH 14

The electrochemical, spectroscopic, and isotope labeling experiments result discussed above allow us to propose a detailed chemical decomposition mechanism for $K_3[Fe(CN)_6]$ at pH 14, as summarized in **Scheme 1**. At pH 14, the chemical redox reaction from $K_3[Fe(CN)_6]$ to $K_4[Fe(CN)_6]$ is mainly attributed to the oxidation of the graphite felt electrodes. The O_2 and CO products only have minor contributions (less than 1% for each) to the chemical reduction of $K_3[Fe(CN)_6]$ under investigated conditions. The major products generated from the graphite felt electrodes are carbonate (CO_3^{2-}) and ammonia (NH_3). We believe the nature of N in the carbon electrode comes from polyacrylonitrile, a common precursor used to produce porous electrodes. It is further believed organic nitrile in the carbon electrode needs to be activated by hydroxide before oxidation. Further studies of the reaction nature of carbon electrodes will be pursed in future.

The dissociated CN^- of $K_3[Fe(CN)_6]$ is converted to OCN^- and leads to the irreversible structure change of $K_3[Fe(CN)_6]$. The OCN^- anion can be further hydrolyzed to CO_3^{2-} and ammonia. The formation of OCN^- anion suggests the involvement of OH^-/H_2O as the oxygen donor. It was also noted that the chemical redox reaction between $K_3[Fe(CN)_6]$ and KCN was also examined at pH 7. Even at pH 7, the identical products, $K_4[Fe(CN)_6]$ and KOCN were observed in the IR spectrum (Figure S41, Supporting Information). At pH 7, the OH^-/CN^- exchange is not detectable as the concentration of OH^- is too low to result in ligand exchange.

According to our recent studies on the degradation of ferrocene catholytes.[11] we also studied the photolytic degradation of $K_3[Fe(CN)_6]$ under ambient light conditions. At pH 7 and 14, battery cycling and UV–vis studies revealed that the degradation of $K_3[Fe(CN)_6]$ was even accelerated under ambient light exposure (Figure 2 and Figure S42, Supporting Information). Even at pH 7, 1.7% capacity loss was observed within 300 cycles (Figure 2B, blue curve). Under the ambient light, the formation of red color $Fe(OH)_3$ precipitate was also observed (Figure S43, Supporting Information) and confirmed by EDS studies (Figure S44, Supporting Information).

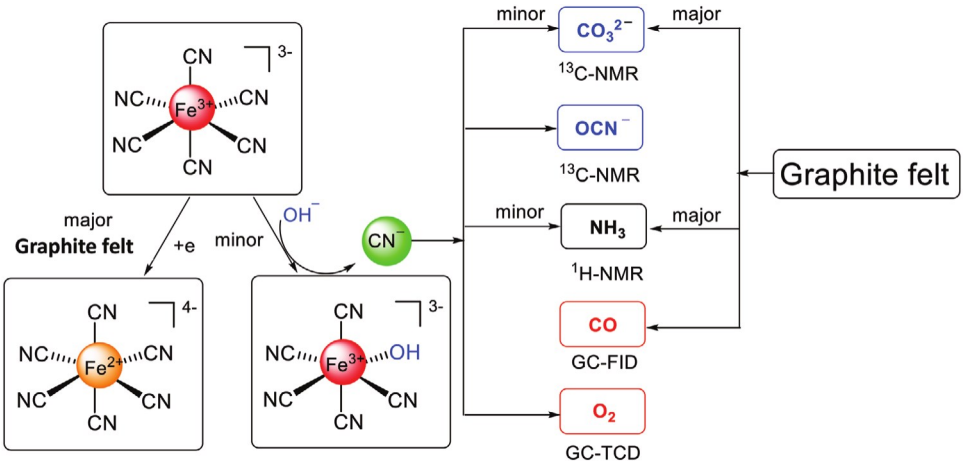

Scheme 1. Proposed degradation mechanisms of $K_3[Fe(CN)_6]$ at pH 14.

The gained mechanistic understanding elucidates the different cycling performances of the $K_4[Fe(CN)_6]/K_3[Fe(CN)_6]$ half cells at different pH conditions. Thus, $K_4[Fe(CN)_6]$ and $K_3[Fe(CN)_6]$ are best used as catholytes under pH-neutral and dark conditions. The presented mechanistic studies also explained the use of excess, mixed $K_4[Fe(CN)_6]/K_3[Fe(CN)_6]$ catholytes in the reported alkaline organic redox flow batteries.[6–9,17] In addition, our results suggest that a balanced half-cell is a reliable configuration to evaluate the cycling stability of a redox-active electrolyte in future studies (Figure 1A,D). Unbalanced half-cell studies are still valuable in detecting which state between a charge state and a discharged state is more susceptible to chemical degradation. However, unbalanced half-cell studies should not be used alone to evaluate the cycling stability of a redox-active electrolyte as it can be misleading by masking the chemical redox degradation as seen in the volume unbalanced $K_4[Fe(CN)_6]/K_3[Fe(CN)_6]$ half-cell.

3. Conclusions

In summary, a suite of battery and spectroscopic studies revealed a detailed degradation mechanism of $K_3[Fe(CN)_6]$ at strong alkaline conditions. The capacity loss of $K_3[Fe(CN)_6]$ is mainly attributed to the chemical reduction of $K_3[Fe(CN)_6]$ to $K_4[Fe(CN)_6]$ by graphite felt. In addition, $K_3[Fe(CN)_6]$ also undergoes slow but irreversible CN ligand dissociation and subsequent degradation reactions. This mechanistic study unequivocally confirms that $K_4[Fe(CN)_6]$ is best used as a catholyte at pH neutral or near neutral conditions instead of strong alkaline conditions. In addition, the balanced half-cell technology should be used to evaluate the cycling stability of a redox-active electrolyte. Finally, the fundamental insights gained in this work will benefit mechanistic studies and molecular designs of other redox-active electrolytes of redox flow batteries for scalable energy storage.

Supporting Information

Supporting Information is available from the Wiley Online Library or from the author.

Acknowledgements

The authors thank National Science Foundation (Career Award, Grant No. 1847674), a Utah State University faculty startup fund, and Utah Science Technology and Research initiative (USTAR) research award for supporting the flow battery project. M.H. and Q.W. are grateful for the China Scholarship Council (CSC) scholarship sponsored by CSC abroad studying program to support their graduate study at Utah State University. The authors acknowledge that the NMR studies are supported by National Science Foundation's Major Research Instrumentation program (Grant No. 1429195).

Conflict of Interest

The authors declare no conflict of interest.

Data Availability Statement

The data that support the findings of this study are available in the supplementary material of this article.

Keywords

energy storage, ferrocyanide electrolytes, redox flow batteries

Received: November 5, 2022
Revised: January 25, 2023
Published online: March 15, 2023

[1] J. Luo, B. Hu, M. Hu, Y. Zhao, T. L. Liu, *ACS Energy Lett.* **2019**, *4*, 2220.
[2] P. Leung, A. A. Shah, L. Sanz, C. Flox, J. R. Morante, Q. Xu, M. R. Mohamed, C. Ponce de León, F. C. Walsh, *J. Power Sources* **2017**, *360*, 243.
[3] J. Luo, B. Hu, C. Debruler, T. L. Liu, *Angew. Chem., Int. Ed.* **2018**, *57*, 231.
[4] C. DeBruler, B. Hu, J. Moss, J. Luo, T. L. Liu, *ACS Energy Lett.* **2018**, *3*, 663.
[5] C. DeBruler, B. Hu, J. Moss, X. Liu, J. Luo, Y. Sun, T. L. Liu, *Chem* **2017**, *3*, 961.

[6] M. Wu, Y. Jing, A. A. Wong, E. M. Fell, S. Jin, Z. Tang, R. G. Gordon, M. J. Aziz, *Chem* **2020**, *6*, 1432.
[7] D. G. Kwabi, K. Lin, Y. Ji, E. F. Kerr, M.-A. Goulet, D. De Porcellinis, D. P. Tabor, D. A. Pollack, A. Aspuru-Guzik, R. G. Gordon, M. J. Aziz, *Joule* **2018**, *2*, 1894.
[8] A. Hollas, X. Wei, V. Murugesan, Z. Nie, B. Li, D. Reed, J. Liu, V. Sprenkle, W. Wang, *Nat. Energy* **2018**, *3*, 508.
[9] C. Zhang, Z. Niu, S. Peng, Y. Ding, L. Zhang, X. Guo, Y. Zhao, G. Yu, *Adv. Mater.* **2019**, *31*, 1901052.
[10] B. Hu, C. DeBruler, Z. Rhodes, T. L. Liu, *J. Am. Chem. Soc.* **2017**, *139*, 1207.
[11] J. Luo, M. Hu, W. Wu, B. Yuan, T. L. Liu, *Energy Environ. Sci.* **2022**, *15*, 1315.
[12] J. Yu, M. Salla, H. Zhang, Y. Ji, F. Zhang, M. Zhou, Q. Wang, *Energy Storage Mater.* **2020**, *29*, 216.
[13] B. Hu, M. Hu, J. Luo, T. L. Liu, *Adv. Energy Mater.* **2022**, *12*, 2102577.
[14] Y. Liu, M.-A. Goulet, L. Tong, Y. Liu, Y. Ji, L. Wu, R. G. Gordon, M. J. Aziz, Z. Yang, T. Xu, *Chem* **2019**, *5*, 1861.
[15] J. Luo, B. Hu, C. Debruler, Y. Bi, Y. Zhao, B. Yuan, M. Hu, W. Wu, T. L. Liu, *Joule* **2019**, *3*, 149.
[16] J. Luo, A. P. Wang, M. Hu, T. L. Liu, *MRS Energy Sustainability* **2022**, *9*, 1.
[17] B. Hu, T. L. Liu, *Science* **2021**, *372*, 788.
[18] J. Luo, A. Sam, B. Hu, C. DeBruler, X. Wei, W. Wang, T. L. Liu, *Nano Energy* **2017**, *42*, 215.
[19] T. Páez, A. Martínez-Cuezva, J. Palma, E. Ventosa, *J. Power Sources* **2020**, *471*, 228453.
[20] M.-A. Goulet, M. J. Aziz, *J. Electrochem. Soc.* **2018**, *165*, A1466.
[21] M. Hu, A. P. Wang, T. Liu, *ChemRxiv* **2022**, https://doi.org/10.26434/chemrxiv-2022-lqms7-v3.
[22] E. Fell, D. De Porcellinis, V. Gutierrez-Venegas, R. Gordon, S. Granados-Focil, M. Aziz, *ChemRxiv* **2022**, https://doi.org/10.26434/chemrxiv-2022-zl7l6.
[23] E. Gail, S. K. Gos, R. , J. Lorösch, A. Rubo, M. Sauer, R. Kellens, J. Reddy, N. Steier, *Cyano Compounds, Inorganic, Ullmann's Encyclopedia of Industrial Chemistry*, John Wiley & Sons, New York **2011**.
[24] B. Adams, R. P. Hollandsworth, B. D. Webber, in *A Technical Report by Lockheed Palo Alto Research Laboratory*, Lockheed Missiles and Space Co., Palo Alto, CA **1979**.